

HYBRID STAR MODELS IN THE LIGHT OF NEW MULTI-MESSENGER DATA

JIA JIE LI¹, ARMEN SEDRAKIAN^{2,3}, MARK ALFORD⁴

¹School of Physical Science and Technology, Southwest University, Chongqing 400715, China; jjajieli@swu.edu.cn

²Frankfurt Institute for Advanced Studies, D-60438 Frankfurt am Main, Germany; sedrakian@fias.uni-frankfurt.de

³Institute of Theoretical Physics, University of Wrocław, 50-204 Wrocław, Poland

⁴Department of Physics, Washington University, St. Louis, MO 63130, USA; alford@physics.wustl.edu

Draft version January 5, 2024

ABSTRACT

Recent astrophysical mass inferences of compact stars (CSs) HESS J1731-347 and PSR J0952-0607, with extremely small and large masses respectively, as well as the measurement of the neutron skin of Ca in the CREX experiment challenge and constrain the models of dense matter. In this work, we examine the concept of hybrid stars - objects containing quark cores surrounded by nucleonic envelopes - as models that account for these new data along with other (multimessenger) inferences. We employ a family of 81 nucleonic equations of state (EoSs) based on covariant density functional with variable skewness and slope of symmetry energy at saturation density and a constant speed-of-sound EoS for quark matter. For each nucleonic EoS, a family of hybrid star EoS is generated by varying the transition density from nucleonic to quark matter, the density jump at the transition, and the speed-of-sound. These models are tested against the data from GW170817 and J1731-347, which favor low-density soft EoS and PSR J0592-0607 and J0740+6620, which require high-density stiff EoS. We then examine the occurrence of twin configurations and quantify the ranges of masses and radii that they can possess. It is shown that including J1731-347 data favors EoS models which predict low-mass twin stars with masses $M \lesssim 1.3 M_{\odot}$ that can be realized if the deconfinement transition density is low. If combined with a large speed-of-sound in quark matter such models allow for maximum masses of hybrid stars in the range 2.0-2.6 M_{\odot} .

Keywords: Compact objects (228); Neutron stars (1108); Nuclear astrophysics (1129); High energy astrophysics (739)

1. INTRODUCTION

Although the concepts of quark stars and hybrid stars containing a quark core enclosed in a nucleonic envelope were proposed long ago and have been intensively studied over the following decades (for reviews, see [Alford et al. \(2008\)](#); [Anglani et al. \(2014\)](#); [Baym et al. \(2018\)](#); [Sedrakian \(2023\)](#)), they remain at the forefront of the exploration of superdense matter and compact stars (CSs). They may arise through the onset of a first-order phase transition between the nucleonic and quark phases, in which case a new branch of stellar equilibria populated by stable hybrid stars arise. One intriguing aspect of hybrid stars is the existence of twin configurations, i.e., two stars that possess the same mass but different radii, whereby the larger star consists entirely of nucleonic matter, while the more compact star is a hybrid star ([Glendenning & Kettner 2000](#); [Zdunik & Haensel 2013](#); [Benic et al. 2015](#); [Alford & Sedrakian 2017](#); [Alvarez-Castillo et al. 2019](#); [Blaschke et al. 2020](#); [Christian & Schaffner-Bielich 2022](#); [Li et al. 2023a](#)). The study of hybrid stars and their twin configurations continues to be an active area of research, with ongoing efforts to explore their properties and to investigate potential observational signatures that could distinguish them from hadronic CSs (see [Alford et al. 2005](#); [Bonanno & Sedrakian 2012](#); [Masuda et al. 2013](#); [Klähn et al. 2013](#); [Christian et al. 2019](#); [Malfatti et al. 2020](#); [Li et al. 2020](#); [Tan et al. 2020, 2022](#); [Brodie & Haber 2023](#); [Tsaloukidis et al. 2023](#), and references therein).

In recent years, observations of CSs have reached unprecedented levels of precision, providing valuable constraints on the EoS of stellar matter and its composition. Among these constraints, the most interesting ones are depicted in Figure 1.

These include:

- (a) The most massive pulsar PSR J0740+6620 ([Fonseca et al. 2021](#)), which has pushed the maximum mass of CSs to 2.0 M_{\odot} .
- (b) The simultaneous mass and radius measurements for PSR J0030+0451 ([Riley et al. 2019](#); [Miller et al. 2019](#)) and J0740+6620 ([Riley et al. 2021](#); [Miller et al. 2021](#)) extracted from X-ray observations using the NICER instrument.
- (c) The detection of gravitational waves from the binary CS merger event GW170817 ([Abbott et al. 2019](#)), which provides us with an estimate of the tidal deformability of the binary that can further yield constraints on the radii of the individual components.
- In addition to these well-established constraints, some more speculative results have been reported very recently:
 - (d) The companion of the “black widow” pulsar PSR J0952-0607 (the second fastest known spinning CS with a frequency of 707 Hz) has been detected in the Milky Way Galaxy, with a mass estimate of $M = 2.35^{+0.17}_{-0.17} M_{\odot}$ (68% credible interval) ([Romani et al. 2022](#)).
 - (e) The X-ray spectrum of the central compact object within the supernova remnant HESS J1731-347 was modeled and in combination with the distance estimates from Gaia observations yielded a very low mass of $M = 0.77^{+0.20}_{-0.17} M_{\odot}$ and a relatively small radius of $R = 10.4^{+0.86}_{-0.78}$ km (68% credible interval) ([Doroshenko et al. 2022](#)).

Given these new (albeit somewhat speculative) observations, it is worthwhile to take a fresh look at the concept of a hybrid star by allowing for a broad range of admissible parameter space within models that have been tested on a more limited set of observations. In the present work, we imple-

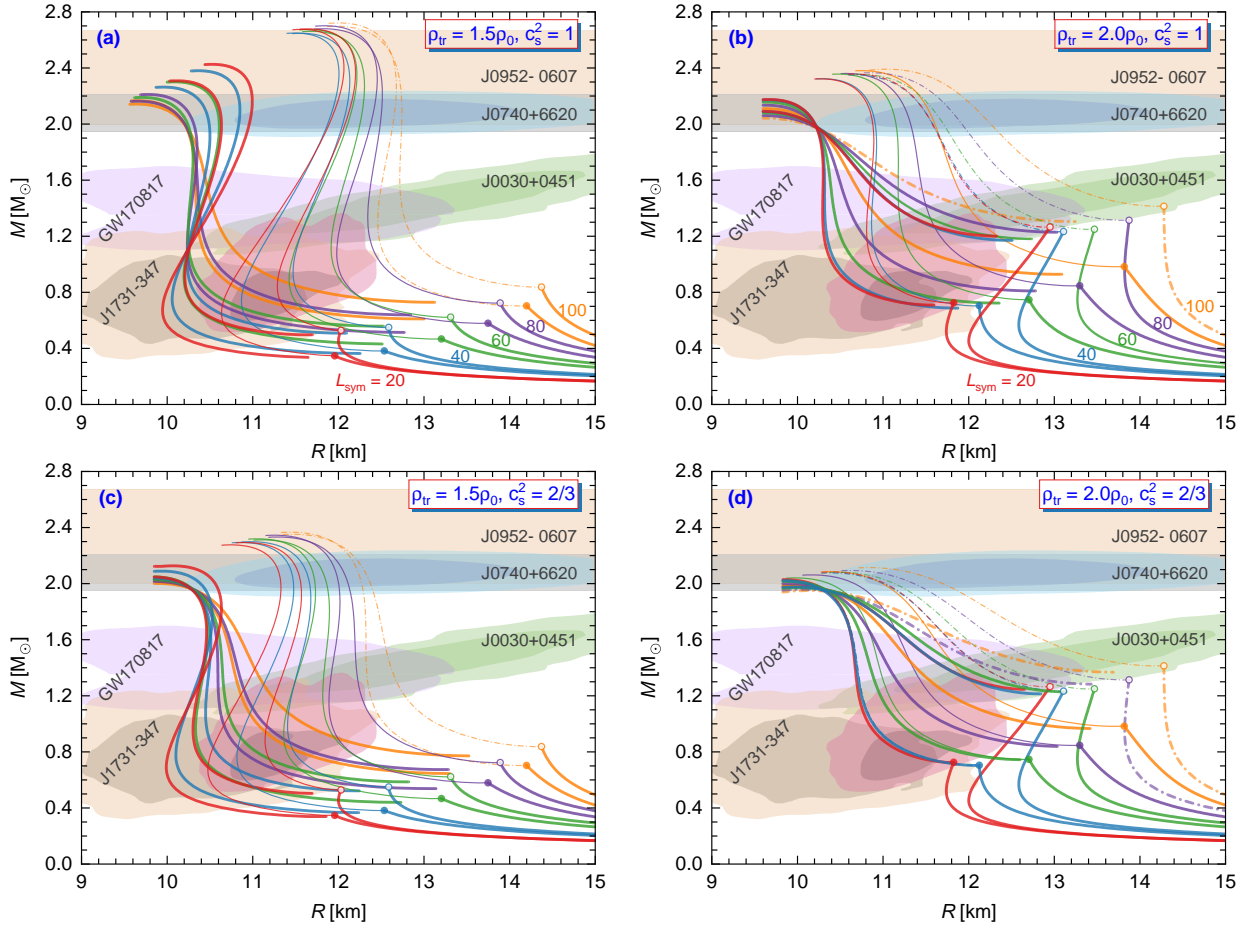


Figure 1. Mass-radius relations for hybrid EoSs with $\rho_{\text{tr}} = 1.5\rho_0$ and $2.0\rho_0$, for $c_s^2 = 1$ and $2/3$ in the quark phase. In each panel, the hybrid EoSs are built upon nucleonic models grouped by $L_{\text{sym}} = 20, 40, 60, 80$ and 100 MeV; for each, Q_{sat} is set to -600 and 1000 MeV. The circle on each curve denotes the configuration with central density ρ_{tr} ; lines ending with a filled circle are for the isoscalar-soft nucleonic model with $Q_{\text{sat}} = -600$ MeV and lines ending with an empty circle are for the isoscalar-stiff one with $Q_{\text{sat}} = 1000$ MeV. Observational constraints from multi-messenger astronomy are shown for comparison (note there are two overlapping regions for HESS J1731-347 (Doroshenko et al. 2022)). For each nucleonic EoS, thick lines show the hybrid models with a maximum energy jump that yields twin configurations and a branch passing through the 95% confidence region for the mass-radius constraints for PSR J0740+6620 and J0030+0451. The thin lines show the model with a critical value of $\Delta\varepsilon$ for which a higher value leads a disconnected mass-radius curve. Solid lines represent models that are satisfying all constraints, while dash-dotted lines show those failing for J1731-347.

ment such a program for the construction of hybrid EoSs and apply filtering to extract the range of EoS that is consistent with the current data. Our further focus is on twin stars and their compatibility with the aforementioned multi-messenger information after the inclusion of extreme domains of mass mentioned above in the analysis.

2. HYBRID MODELS

To describe low-density matter, we use a covariant density functional of nuclear matter in which baryons are coupled to mesons with density-dependent couplings (Typel & Wolter 1999; Oertel et al. 2017; Sedrakian et al. 2023). The nuclear matter properties are conveniently assessed using the coefficients of Taylor expansion of energy density with respect to the baryon density and isospin asymmetry at the saturation density ρ_0 . The low-order coefficients, the saturation energy E_{sat} , compressibility K_{sat} , and symmetry energy J_{sym} are either strongly constrained or have no noticeable impact on the gross properties (e.g., mass, radius, deformability, etc.) of CSs (Margueron et al. 2018; Li & Sedrakian 2019).

Here we adopt a family of nucleonic EoS consisting of 81 EoS which share the same low-order coefficients as the original DDME2 parameterization (Lalazissis et al. 2005), but have alternative density-dependence of the couplings, thus,

resulting in different high-order coefficients (Li & Sedrakian 2023). Specifically, the skewness coefficient for symmetric matter (characterizing the isoscalar sector) varies in the range $-600 \leq Q_{\text{sat}} \leq 1000$ MeV and the slope parameter of the symmetry energy (characterizing the isovector sector) varies in the range $20 \leq L_{\text{sym}} \leq 100$ MeV. Note that values of Q_{sat} and L_{sym} control, respectively, the high- and intermediate-density behaviors of the nucleonic EoS, thereby influencing the maximum mass of static nucleonic stars and the radius of the canonical-mass star (Margueron et al. 2018; Li & Sedrakian 2019). The value of L_{sym} , commonly considered to be close to 60 MeV, has been challenged by the recent analyses of the neutral weak form factor of ^{48}Ca in the CREX experiment, which suggests rather low values of $L_{\text{sym}} = 20 \pm 30$ MeV (Adhikari et al. 2022; Lattimer 2023). This can be contrasted to the values of $L_{\text{sym}} = 106 \pm 37$ MeV obtained by some groups via the analysis of the neutron skin thickness of ^{208}Pb in the PREX-II experiment (Adhikari et al. 2021).

The quark phase is described by the constant sound speed (CSS) parametrization (Zdunik & Haensel 2013; Alford et al. 2013)

$$p(\varepsilon) = \begin{cases} p_{\text{tr}}, & \varepsilon_{\text{tr}} < \varepsilon < \varepsilon_{\text{tr}} + \Delta\varepsilon, \\ p_{\text{tr}} + c_s^2 [\varepsilon - (\varepsilon_{\text{tr}} + \Delta\varepsilon)], & \varepsilon_{\text{tr}} + \Delta\varepsilon < \varepsilon, \end{cases} \quad (1)$$

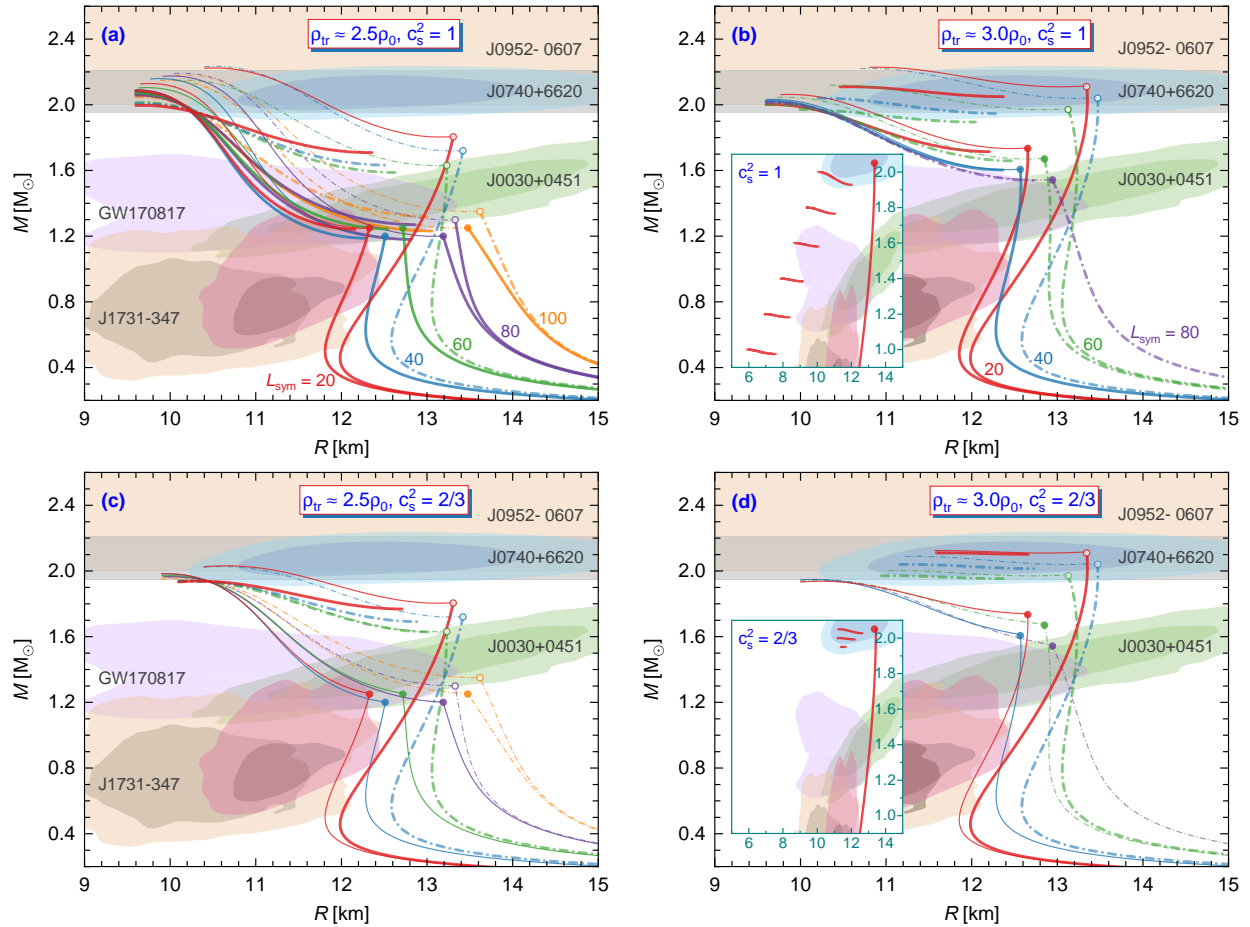


Figure 2. Mass-radius relations for hybrid EoSs with $\rho_{\text{tr}} \approx 2.5\rho_0$ and $3.0\rho_0$, for $c_s^2 = 1$ and $2/3$ in the quark phase. In each panel, the hybrid EoSs are constructed from nucleonic models grouped by $L_{\text{sym}} = 20, 40, 60, 80$ and 100 MeV; for each, Q_{sat} is chosen such that the resultant mass-radius curve passes through the 95% confidence region for HESS J1731-347 (solid lines) or GW170817 (dash-dotted lines), respectively. The circle on each curve denotes the configurations with central density ρ_{tr} . Thick lines show the hybrid models with a maximum $\Delta\varepsilon$ that yield twin configurations and a branch passing through the 95% confidence region for PSR J0740+6620. Thin lines show the models with a connected mass-radius curve with a critical value of $\Delta\varepsilon$ set by the constraint for J0740+6620 or appearance of twin configurations. The inset illustrates hybrid EoSs built upon an isoscalar-stiff nucleonic model for the case $M_{\text{max}}^{\text{Q}} \leq M_{\text{max}}^{\text{H}}$ which yields ultra-compact configurations for the case $c_s^2 = 1$. Solid lines represent models satisfying all constraints, while dash-dotted lines show those failing for J1731-347.

where p_{tr} is the pressure and ε_{tr} is the energy density at the phase transition from nucleonic to quark matter at zero temperature and nucleonic density ρ_{tr} ; $\Delta\varepsilon$ is the energy discontinuity and c_s is the sound speed in the quark phase. The first-order phase transition described by this EoS leads to a new stable branch populated by hybrid stars which may or may not be separated from the nucleonic branch by an instability region. Furthermore, for a range of parameters, this leads to the phenomenon of twin configurations — two stable CSs that have identical masses but different radii and consequently, tidal deformabilities (Alford et al. 2013; Benic et al. 2015; Paschalidis et al. 2018; Alvarez-Castillo et al. 2019; Christian et al. 2019; Montana et al. 2019; Christian & Schaffner-Bielich 2021). In this work, we adopt two values of c_s^2 : the maximally stiff EoS with $c_s^2 = 1$ (in natural units) allows us to explore the limits of ranges of masses and radii accessible to models of the type considered in this work; see also Tsakoulidis et al. (2023). The alternative value $c_s^2 = 2/3$ is intermediate between the maximally stiff and the asymptotically high-density value $c_s^2 = 1/3$ corresponding to a conformally symmetric quark phase. Other values of c_s^2 have been considered very recently by several authors (Brodie & Haber 2023; Sagun et al. 2023) in the context of HESS J1731-347 for al-

ternate nucleonic EoSs.

3. COMPUTATIONAL SCHEME

To cover the parameter space of our model, we choose from the family of 81 nucleonic EoS models given in Li & Sedrakian (2023) a subset which are identified by the values of Q_{sat} and L_{sym} . We then choose the values for $\rho_{\text{tr}} = 1.5, 2.0, 2.5, 3.0\rho_0$ to match these nucleonic EoS to quark matter EoS, for a magnitude of the density jump $\Delta\varepsilon$ and sound speed $c_s^2 = 2/3$ or 1.

For each EoS in our collection, we solve the Tolman-Oppenheimer-Volkoff equations for static and spherically symmetric stellar objects. If all the mass and radius ranges of astronomical data are intersected by a sequence corresponding to a particular EoS it is accepted, otherwise it is rejected. More specifically, we consider the set of constraints (a)-(c) listed in the Introduction, i.e., those based on NICER inferences of mass and radius for J0030+0451 and J0740+6620, GW170817 inference of radii and masses in the binary CS merger, and radio-wave measurements of the mass of J0740+6620. We then supplement these by the mass and radius of J1731-347 and the mass of J0952-0607. Note that, if we assume that uniform rotation, the increase of mass of the maximum-mass configuration due to the rotation of 707 Hz is

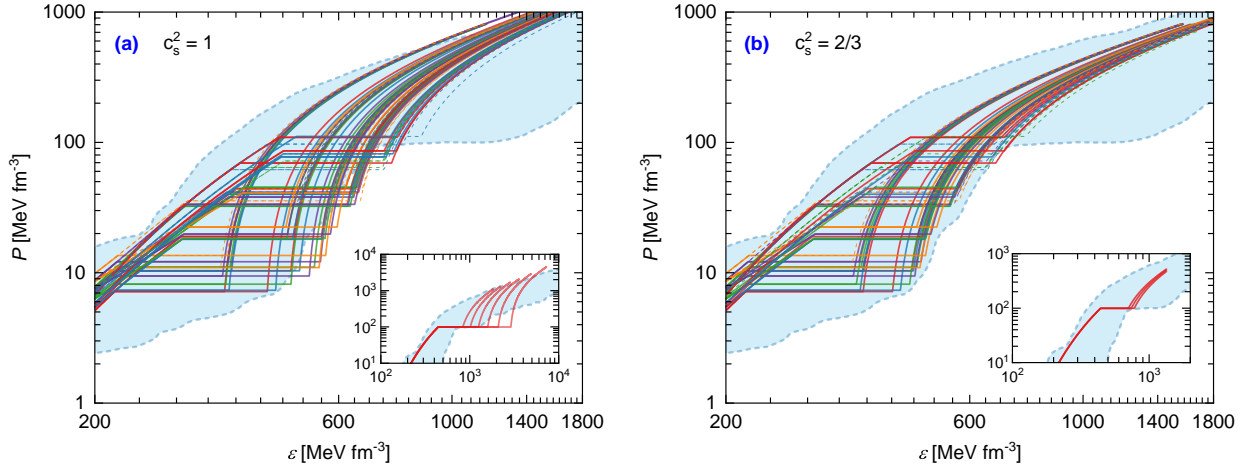


Figure 3. EoS collection utilized in the work. Solid thick lines represent models that satisfy all constraints, while dashed thin lines show those that fail for HESS J1731-347. The blue regions display the allowed region of EoS from [Annala et al. \(2022\)](#), which includes EoS mimicking first-order phase transitions. Insets show EoS that give rise to ultra-compact stars.

about of $0.05 M_{\odot}$. Therefore, the lower limit on the mass of J0952-0607 is about the same as that of J0740+6620 at a 95% confidence level. The parameters for quark EoS, p_{tr} and $\Delta\epsilon$, can be transformed into observational properties of CSs, i.e., the maximum mass of the nucleonic branch $M_{\text{max}}^{\text{H}}$ and that of the hybrid branch $M_{\text{max}}^{\text{Q}}$, respectively, in the M - R diagram ([Li et al. 2023b](#)). We further introduce the minimal mass in the hybrid branch, denoted as $M_{\text{min}}^{\text{Q}}$, which we shall use for assessing the range of mass where twin configurations exist.

4. ANALYSIS OF THE RESULTS

Figures 1 and 2 show the M - R diagrams for hybrid EoS models where the nucleonic EoS is specified by values of Q_{sat} and L_{sym} and the quark matter EoS is specified by the sound speed value $c_s^2 = 1$ and $2/3$. Figure 1 is for lower transition densities $\rho_{\text{tr}} = 1.5$ or $2.0\rho_0$; Figure 2 is for higher transition densities $\rho_{\text{tr}} = 2.5$ or $3.0\rho_0$. The isovector properties of nucleonic EoS are measured by the value of L_{sym} . Consider first the isovector-soft ($L_{\text{sym}} = 20$ MeV) EoSs, which contain members that are consistent with astrophysical constraints at the 95% confidence level for any of the chosen parameters shown in panels of Figures 1 and 2. It is seen that as the transition density increases in the considered range 1.5 - $3.0\rho_0$ the masses of twin stars increase as well. A larger speed-of-sound allows the hybrid branch to stretch to the region of smaller radii, and more generally to cover a broader range, as can be seen from the ultra-compact members shown in the insets in panels (b, d) of Figure 2. These models can be contrasted with the isovector-stiff ($L_{\text{sym}} = 80$ MeV) EoSs. In this case, the transition to quark matter needs to occur at a sufficiently low density $\rho_{\text{tr}} \lesssim 2.0\rho_0$, to satisfy the constraints imposed by HESS J1731-347 and GW170817, as displayed in Figure 1. Furthermore, compatibility with the large radius of PSR J0740+6620 is achieved for relatively small energy density discontinuity at the phase transition. The resulting sequences satisfy the two-solar mass constraint because the maximum of the hybrid branch $M_{\text{max}}^{\text{Q}} \sim 2.0 M_{\odot}$, which is also the maximum mass for the entire sequences. In this case, only low-mass twin configurations appear that are consistent with astrophysical constraints.

Figure 3 shows the high-density portion of all the EoS used in this work, i.e., including those that fail to account for HESS J1731-347. The EoS of ultra-compact stars, with radii in the range $6 \leq R \leq 10$ km and much higher central densities, is

separated in the insets. It is seen that the addition of J1731-347 does not change the range of allowed EoS and that the high-density range covered by our collection is broadly compatible with the one deduced in [Annala et al. \(2022\)](#) by imposing current astrophysical constraints on a very large randomly generated ensemble of physics-agnostic EoS covering the intermediate density range. We also note that the low-density range of the EoS, which can be found in [Li & Sedrakian \(2023\)](#), is consistent with the low-density microscopic (chiral) EoS, as presented in [Annala et al. \(2022\)](#), only for $40 \leq L_{\text{sym}} \leq 60$.

To facilitate the following discussion, we divided the stellar configurations into those where the maximum-mass star is on the hybrid branch (case A) and those where the maximum-mass star is on the nucleonic branch (case B). This type of classification has been considered previously; case A was studied in [Li et al. \(2021\)](#) and [Christian & Schaffner-Bielich \(2022\)](#) and case B in [Li et al. \(2023a\)](#).

Case A: Figure 4 summarizes the contours representing the ranges of mass and radius that characterize twin configurations for hybrid EoS models with $M_{\text{max}}^{\text{H}} \leq M_{\text{max}}^{\text{Q}}$ for $c_s^2 = 1$. Filled symbols indicate models that satisfy astrophysical constraints, while empty symbols represent models that do not. The color of the square shows the range of mass or radius over which twins can be found. The case $c_s^2 = 2/3$ shows the same trends but the ranges of masses and radii are significantly narrower. The shape of the sequences in Case A dictates that the range of masses where twin configurations exist is defined as $\Delta M_{\text{twin}} = M_{\text{max}}^{\text{H}} - M_{\text{min}}^{\text{Q}}$. Then, the differences in radii ΔR_{twin} for twin configurations is determined by comparing the radius of $M_{\text{max}}^{\text{H}}$ nucleonic star to that of the hybrid counterpart with an identical mass. It can be observed from Figures 1 and 2 that this is also the maximal radius difference for a hybrid EoS predicting twin configurations. A lesson that we learn from Figure 4 is that the possible combinations $M_{\text{max}}^{\text{Q}}$ and $M_{\text{max}}^{\text{H}}$ for which twin configurations exist is large for the isovector-soft nucleonic model [(panel (a))] and is small for the isovector-stiff model [(panel (c))]. Also these two cases predict different $M_{\text{max}}^{\text{Q}}$ and $M_{\text{max}}^{\text{H}}$ for which the largest range of masses $\leq 0.2 M_{\odot}$ (shown by dark squares) is achieved. The corresponding values of ΔR_{twin} shown in panels (b, d) indicate that the largest difference between the twin radii is achieved for sequences that have both maxima around the two-solar mass. The twins with $\Delta R_{\text{twin}} \sim 4$ - 5 km correspond to ultra-

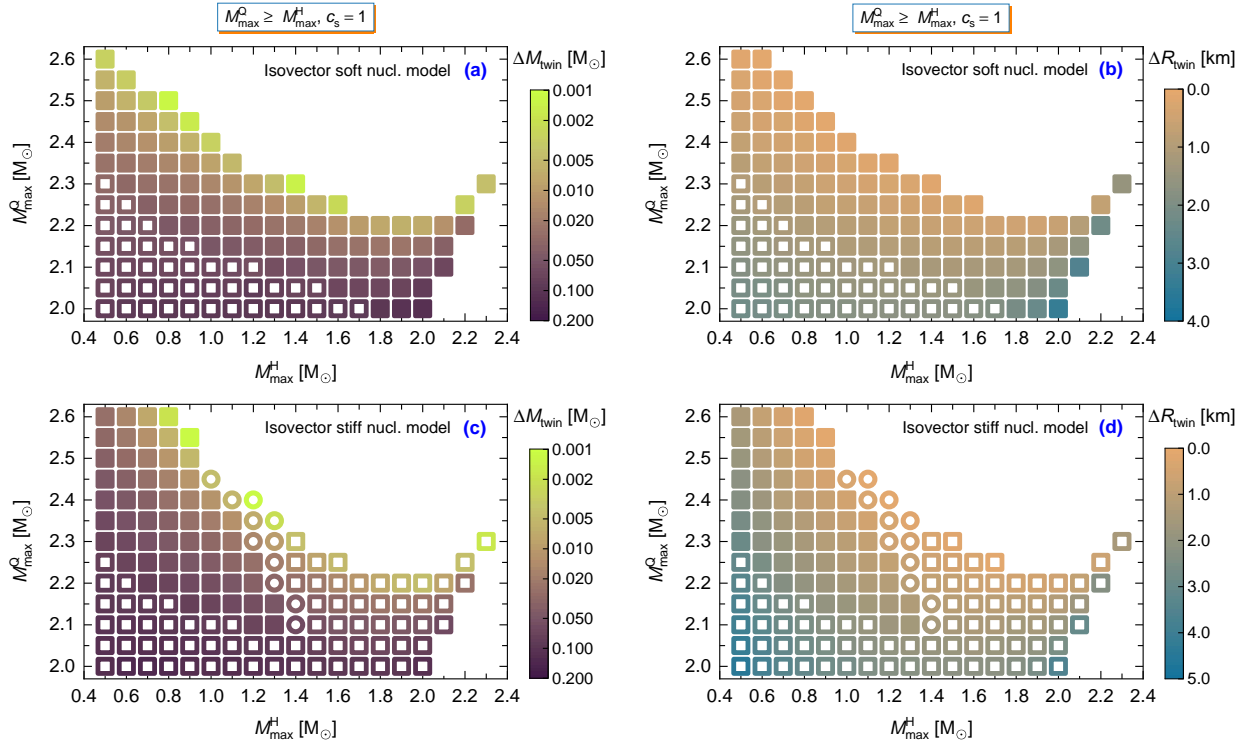


Figure 4. Ranges of mass and radius that characterize twin configurations for the case A, i.e., $M_{\max}^Q \geq M_{\max}^H$. In panels (a, b) the hybrid EoS models ($c_s^2 = 1$) are built using an isovector-soft nucleonic model ($Q_{\text{sat}} = 800$, $L_{\text{sym}} = 20$ MeV), while in panels (c, d) - using an isovector-stiff nucleonic model ($Q_{\text{sat}} = 800$, $L_{\text{sym}} = 80$ MeV). Panels (a, c) show the mass ranges of twins ΔM_{twin} using color coding. Panels (b, d) do the same but for the radii of twin configurations ΔR_{twin} . By open squares, we show the models that are ruled out by combined observational constraints, whereas by open circles we show those that are excluded by HESS J1731-347 data.

compact hybrid stars discussed earlier by us (Li et al. 2023a).

Case B: Figure 5 summarizes the ranges of masses and radii that characterize twin configurations for hybrid EoS models in the case $M_{\max}^Q \leq M_{\max}^H$, for $c_s^2 = 1$. Here the range of masses is defined $\Delta M_{\text{twin}} = M_{\max}^Q - M_{\min}^Q$, and the differences in radii ΔR_{twin} is extracted from the radius of M_{\max}^Q hybrid star and its nucleonic twin. For such cases, as illustrated in the insets of Figure 2, we require the nucleonic branch passing through all the 95% confidence regions of constraints, this

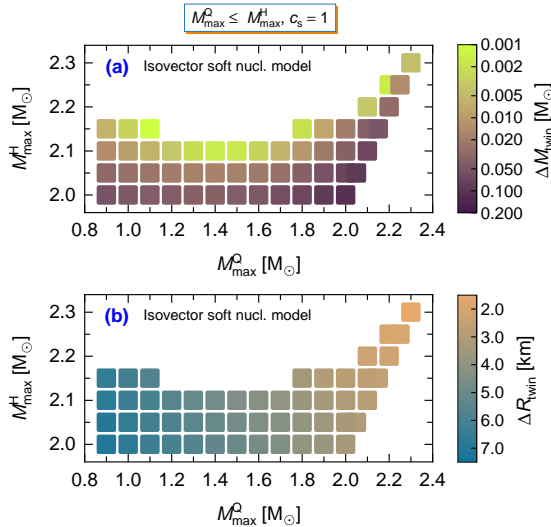


Figure 5. Same as in Figure 4 but for the case B corresponding to $M_{\max}^Q \leq M_{\max}^H$. The hybrid EoS models ($c_s^2 = 1$) are built upon an isovector-soft nucleonic model ($Q_{\text{sat}} = 800$, $L_{\text{sym}} = 20$ MeV). Ultra-compact configurations having large ΔR_{twin} are present only for models with $M_{\max}^H \approx 2.0$ - $2.15 M_{\odot}$.

can be achieved only for isovector-soft models. It is seen that ultra-compact configurations with radii $6 \leq R \leq 10$ km, associated with large values of ΔR_{twin} , are present only for models with $M_{\max}^H \approx 2.0$ - $2.15 M_{\odot}$. These ultra-compact members studied in more detail in (Li et al. 2023a) together with those appearing in the case A offer an alternative to strange stars, which up until recently were considered as the only possible objects with small radii (of the order of 6–9 km) (see Bombaci et al. 2021, and references therein). It is worthwhile also to mention that the mass values found for twins in this case are well within the range of mass obtained for PSR J0592-0607 at a 95% confidence level (Romani et al. 2022).

5. CONCLUSIONS

In this work, we investigated the consistency of the hybrid star models with the current astrophysical and laboratory data and explored the range of parameters that lead to twin stars. To do so, we employed a recently constructed family of nucleonic EoSs parametrized by the Q_{sat} and L_{sym} parameters of the Taylor expansion of the energy density of nucleonic matter. This was then combined with a CSS parameterization of the quark matter EoS for a range of values of the transition density, energy density jump, and sound speed. We have identified two classes of models with low and high transition densities (as shown in Figures 1 and 2, respectively) that are consistent with the current data. This is achieved through a compromise between the requirement for a soft EoS at low densities, driven by the data from GW170817, and the need for stiff EoS at high densities to account for the radio-astronomy data for PSR J0592-0607 and J0740+6620. The ranges of parameters of twin configurations that are allowed by our hybrid models were found as shown in Figures 4 and 5. Notably,

the data from HESS J1731-347 supports the existence of low-mass twin configurations with masses $M \lesssim 1.3 M_{\odot}$, regardless of the chosen nucleonic EoS, but it requires a low value for the transition density. These hybrid models also allow for maximum masses M_{\max}^{Ω} ranging from 2.0-2.6 M_{\odot} depending on the value of the sound speed in quark matter. In addition, ultra-compact configurations, which lie outside the constraints imposed by GW170817 and J1731-347, emerge for isoscalar-stiff nucleonic EoS models and for large speed-of-sound $c_s = 1$ in the case where the nucleonic branch extends up to 2.0-2.15 M_{\odot} .

In conclusion, the current astrophysical and nuclear physics data do not rule out hybrid stars, and leave room for hybrid-nucleonic mass twins if a strong first-order phase transition occurs in dense matter for reasonable values of nucleonic isoscalar and isovector characteristics. It is even plausible to argue that all the stars with observational information we have considered in this study are hybrid configurations. But this does not exclude the possibility that current observational data is accounted for by the nucleonic branch of hybrid sequences, whereas the hybrid branch lies outside of ranges currently covered, as would be the case for ultra-compact members of sequences.

ACKNOWLEDGEMENTS

J. L. acknowledges the support of the National Natural Science Foundation of China (Grant No. 12105232), the Fundamental Research Funds for the Central Universities (Grant No. SWU-020021), and by the Venture & Innovation Support Program for Chongqing Overseas Returnees (Grant No. CX2021007). A. S. acknowledges the DFG No. SE 1836/5-2 and the Polish NCN Grant No. 2020/37/B/ST9/01937 at Wrocław University. M. A. is partly supported by the U.S. Department of Energy, Office of Science, Office of Nuclear Physics under Award No. DE-FG02-05ER41375.

REFERENCES

- Abbott, B. P., Abbott, R., Abbot, T. D., et al. 2019, *PhRvX*, 9, 011001, doi: [10.1103/PhysRevX.9.011001](https://doi.org/10.1103/PhysRevX.9.011001)
- Adhikari, D., Albataineh, H., Androic, D., et al. 2021, *PhRvL*, 126, 172502, doi: [10.1103/PhysRevLett.126.172502](https://doi.org/10.1103/PhysRevLett.126.172502)
- . 2022, *PhRvL*, 129, 042501, doi: [10.1103/PhysRevLett.129.042501](https://doi.org/10.1103/PhysRevLett.129.042501)
- Alford, M., Braby, M., Paris, M. W., & Reddy, S. 2005, *ApJ*, 629, 969, doi: [10.1086/430902](https://doi.org/10.1086/430902)
- Alford, M., & Sedrakian, A. 2017, *PhRvL*, 119, 161104, doi: [10.1103/PhysRevLett.119.161104](https://doi.org/10.1103/PhysRevLett.119.161104)
- Alford, M. G., Han, S., & Prakash, M. 2013, *PhRvD*, 88, 083013, doi: [10.1103/PhysRevD.88.083013](https://doi.org/10.1103/PhysRevD.88.083013)
- Alford, M. G., Schmitt, A., Rajagopal, K., & Schäfer, T. 2008, *RvMP*, 80, 1455, doi: [10.1103/RevModPhys.80.1455](https://doi.org/10.1103/RevModPhys.80.1455)
- Alvarez-Castillo, D. E., Blaschke, D. B., Grunfeld, A. G., & Pagura, V. P. 2019, *PhRvD*, 99, 063010, doi: [10.1103/PhysRevD.99.063010](https://doi.org/10.1103/PhysRevD.99.063010)
- Anglani, R., Casalbuoni, R., Ciminale, M., et al. 2014, *RvMP*, 86, 509, doi: [10.1103/RevModPhys.86.509](https://doi.org/10.1103/RevModPhys.86.509)
- Annala, E., Gorda, T., Katerini, E., et al. 2022, *PhRvX*, 12, 011058, doi: [10.1103/PhysRevX.12.011058](https://doi.org/10.1103/PhysRevX.12.011058)
- Baym, G., Hatsuda, T., Kojo, T., et al. 2018, *RPPH*, 81, 056902, doi: [10.1088/1361-6633/aaae14](https://doi.org/10.1088/1361-6633/aaae14)
- Benic, S., Blaschke, D., Alvarez-Castillo, D. E., Fischer, T., & Typel, S. 2015, *A&A*, 577, A40, doi: [10.1051/0004-6361/201425318](https://doi.org/10.1051/0004-6361/201425318)
- Blaschke, D., Ayriyan, A., Alvarez-Castillo, D. E., & Grigorian, H. 2020, *Univ*, 6, 81, doi: [10.3390/universe6060081](https://doi.org/10.3390/universe6060081)
- Bombaci, I., Drago, A., Logoteta, D., Pagliara, G., & Vidaña, I. 2021, *PhRvL*, 126, 162702, doi: [10.1103/PhysRevLett.126.162702](https://doi.org/10.1103/PhysRevLett.126.162702)
- Bonanno, L., & Sedrakian, A. 2012, *A&A*, 539, A16, doi: [10.1051/0004-6361/201117832](https://doi.org/10.1051/0004-6361/201117832)
- Brodie, L., & Haber, A. 2023, *PhRvC*, 108, 025806, doi: [10.1103/PhysRevC.108.025806](https://doi.org/10.1103/PhysRevC.108.025806)
- Christian, J.-E., & Schaffner-Bielich, J. 2021, *PhRvD*, 103, 063042, doi: [10.1103/PhysRevD.103.063042](https://doi.org/10.1103/PhysRevD.103.063042)
- Christian, J.-E., & Schaffner-Bielich, J. 2022, *ApJ*, 935, 122, doi: [10.3847/1538-4357/ac75cf](https://doi.org/10.3847/1538-4357/ac75cf)
- Christian, J.-E., Zacchi, A., & Schaffner-Bielich, J. 2019, *PhRvD*, 99, 023009, doi: [10.1103/PhysRevD.99.023009](https://doi.org/10.1103/PhysRevD.99.023009)
- Doroshenko, V., Suleimanov, V., Pühlhofer, G., & Santangelo, A. 2022, *NatAs*, 6, 1444
- Fonseca, E., Cromartie, H. T., Pennucci, T. T., et al. 2021, *ApJL*, 915, L12, doi: [10.3847/2041-8213/ac03b8](https://doi.org/10.3847/2041-8213/ac03b8)
- Glendenning, N. K., & Kettner, C. 2000, *A&A*, 353, L9, <https://arxiv.org/abs/astro-ph/9807155>
- Klähn, T., Łastowiecki, R., & Blaschke, D. B. 2013, *PhRvD*, 88, 085001, doi: [10.1103/PhysRevD.88.085001](https://doi.org/10.1103/PhysRevD.88.085001)
- Lalazissis, G. A., Niksic, T., Vretenar, D., & Ring, P. 2005, *PhRvC*, 71, 024312, doi: [10.1103/PhysRevC.71.024312](https://doi.org/10.1103/PhysRevC.71.024312)
- Lattimer, J. M. 2023, *Particles*, 6, 30, doi: [10.3390/particles6010003](https://doi.org/10.3390/particles6010003)
- Li, J. J., & Sedrakian, A. 2019, *ApJL*, 874, L22, doi: [10.3847/2041-8213/ab1090](https://doi.org/10.3847/2041-8213/ab1090)
- . 2023, *ApJ*, 957, 41, doi: [10.3847/1538-4357/acfa73](https://doi.org/10.3847/1538-4357/acfa73)
- Li, J. J., Sedrakian, A., & Alford, M. 2020, *PhRvD*, 101, 063022, doi: [10.1103/PhysRevD.101.063022](https://doi.org/10.1103/PhysRevD.101.063022)
- . 2021, *PhRvD*, 104, L121302, doi: [10.1103/PhysRevD.104.L121302](https://doi.org/10.1103/PhysRevD.104.L121302)
- . 2023a, *PhRvD*, 107, 023018, doi: [10.1103/PhysRevD.107.023018](https://doi.org/10.1103/PhysRevD.107.023018)
- . 2023b, *ApJ*, 944, 206, doi: [10.3847/1538-4357/acb688](https://doi.org/10.3847/1538-4357/acb688)
- Malfatti, G., Orsaria, M. G., Ranea-Sandoval, I. F., Contrera, G. A., & Weber, F. 2020, *PhRvD*, 102, 063008, doi: [10.1103/PhysRevD.102.063008](https://doi.org/10.1103/PhysRevD.102.063008)
- Margueron, J., Hoffmann Casali, R., & Gulminelli, F. 2018, *PhRvC*, 97, 025806, doi: [10.1103/PhysRevC.97.025806](https://doi.org/10.1103/PhysRevC.97.025806)
- Masuda, K., Hatsuda, T., & Takatsuka, T. 2013, *ApJ*, 764, 12, doi: [10.1088/0004-637X/764/1/12](https://doi.org/10.1088/0004-637X/764/1/12)
- Miller, M. C., Lamb, F. K., Dittmann, A. J., et al. 2019, *ApJL*, 887, L24, doi: [10.3847/2041-8213/ab50c5](https://doi.org/10.3847/2041-8213/ab50c5)
- . 2021, *ApJL*, 918, L28, doi: [10.3847/2041-8213/ac089b](https://doi.org/10.3847/2041-8213/ac089b)
- Montana, G., Tolos, L., Hanauske, M., & Rezzolla, L. 2019, *PhRvD*, 99, 103009, doi: [10.1103/PhysRevD.99.103009](https://doi.org/10.1103/PhysRevD.99.103009)
- Oertel, M., Hempel, M., Klähn, T., & Typel, S. 2017, *RvMP*, 89, 015007, doi: [10.1103/RevModPhys.89.015007](https://doi.org/10.1103/RevModPhys.89.015007)
- Paschalidis, V., Yagi, K., Alvarez-Castillo, D., Blaschke, D. B., & Sedrakian, A. 2018, *PhRvD*, 97, 084038, doi: [10.1103/PhysRevD.97.084038](https://doi.org/10.1103/PhysRevD.97.084038)
- Riley, T. E., Watts, A. L., Bogdanov, S., et al. 2019, *ApJL*, 887, L21, doi: [10.3847/2041-8213/ab481c](https://doi.org/10.3847/2041-8213/ab481c)
- Riley, T. E., Watts, A. L., Ray, P. S., et al. 2021, *ApJL*, 918, L27, doi: [10.3847/2041-8213/ac0a81](https://doi.org/10.3847/2041-8213/ac0a81)
- Romani, R. W., Kandel, D., Filippenko, A. V., Brink, T. G., & Zheng, W. 2022, *ApJL*, 934, L17, doi: [10.3847/2041-8213/ac8007](https://doi.org/10.3847/2041-8213/ac8007)
- Sagun, V., Giangrandi, E., Dietrich, T., et al. 2023, *ApJ*, 958, 49, doi: [10.3847/1538-4357/acfc9e](https://doi.org/10.3847/1538-4357/acfc9e)
- Sedrakian, A. 2023, *Particles*, 6, 713, doi: [10.3390/particles6030044](https://doi.org/10.3390/particles6030044)
- Sedrakian, A., Li, J. J., & Weber, F. 2023, *PrPNP*, 131, 104041, doi: [10.1016/j.pnpnp.2023.104041](https://doi.org/10.1016/j.pnpnp.2023.104041)
- Tan, H., Dore, T., Dexheimer, V., Noronha-Hostler, J., & Yunes, N. 2022, *PhRvD*, 105, 023018, doi: [10.1103/PhysRevD.105.023018](https://doi.org/10.1103/PhysRevD.105.023018)
- Tan, H., Noronha-Hostler, J., & Yunes, N. 2020, *PhRvL*, 125, 261104, doi: [10.1103/PhysRevLett.125.261104](https://doi.org/10.1103/PhysRevLett.125.261104)
- Tsaloukidis, L., Koliogiannis, P. S., Kanakis-Pegios, A., & Moustakidis, C. C. 2023, *PhRvD*, 107, 023012, doi: [10.1103/PhysRevD.107.023012](https://doi.org/10.1103/PhysRevD.107.023012)
- Typel, S., & Wolter, H. H. 1999, *NuPhA*, 656, 331, doi: [10.1016/S0375-9474\(99\)00310-3](https://doi.org/10.1016/S0375-9474(99)00310-3)
- Zdunik, J. L., & Haensel, P. 2013, *A&A*, 551, A61, doi: [10.1051/0004-6361/201220697](https://doi.org/10.1051/0004-6361/201220697)